Contrasted mixing efficiency in energetic versus quiescent regions: Insights from microstructure measurements in the Western Mediterranean Sea

Anda Vladoiu, Pascale Bouruet-Aubertot, Yannis Cuypers, Bruno Ferron, Katrin Schroeder, Mireno Borghini, Stéphane Leizour

Progress in Oceanography
July 2021, Volume 195, Pages 102594 (11p.)
https://doi.org/10.1016/j.pocean.2021.102594
https://archimer.ifremer.fr/doc/00694/80580/

Contrasted mixing efficiency in energetic versus quiescent regions: insights from microstructure measurements in the Western Mediterranean Sea

Vladoiu Anda [1, *], Bouruet-Aubertot Pascale [1], Cuypers Yannis [1], Ferron Bruno [5], Schroeder Katrin [3], Borghini Mireno [4], Leizour Stephane [2]

[1] Sorbonne Université UPMC Paris VI - LOCEAN, France
[2] University of Brest, CNRS, IFREMER, IRD, Laboratoire d'Océanographie Physique et Spatiale, IUEM, Brest, France
[3] CNR-ISMAR, Venice, Italy
[4] CNR-ISMAR, Lerici (SP), Italy
[5] University of Brest, CNRS, IFREMER, IRD, Laboratoire d'Océanographie Physique et Spatiale, IUEM, Brest, France

* Corresponding author : Anda Vladoiu, email address : avladoiu@apl.uw.edu

Abstract :

Microstructure and CTD/LADCP measurements from the Western Mediterranean basin east of revealed two types of dynamical regions (Ferron et al., 2017, Geophysical Research Letters, 44:7845-7854, Ferron et al., 2017), contrasted in terms of current magnitude, vertical shear, stratification and turbulent kinetic energy dissipation rate: energetic regions (Corsica Channel, Egadi Valley and Sicily Channel) and quiescent regions (Ligurian Sea, around Sardinia, and Tyrrhenian Sea). On average, the current speed and the buoyancy frequency in the energetic regions were twice as large as in the quiescent regions, and the vertical shear was five times as large. Turbulence properties inferred from the microstructure measurements were also contrasted, dissipation rates in the energetic regions being two orders of magnitude larger than in the quiescent regions. The present study investigates the variability of the dissipation flux coefficient, a measure of the mixing efficiency, in a rich assortment of dynamical regimes. This dataset covers the full range of turbulence intensities observed in previous studies based on field measurements, direct numerical simulations, and laboratory experiments alike. The dependency of the dissipation flux coefficient as a function of turbulence intensity for the quiescent and energetic regions frames the previously observed lower and upper bounds, respectively. A contrasting behaviour was revealed between the two types of regions. In the quiescent regions, the dissipation flux coefficient linearly decreases on average by one order of magnitude with turbulence intensity increasing by four orders of magnitude. On the other hand, in the energetic regions the dissipation flux coefficient exhibits a nearly constant value over 4 decades of turbulence intensity, before decreasing for very strong turbulence intensities. In contrast with other studies, this dataset shows no relationship between the Richardson number and the dissipation flux coefficient. This may be due to inadequate vertical sampling resolution of the currents, or to the high diversity of sampled turbulent regimes, contrary to previous studies focused on a single type of dynamical region or framework (such as the thermocline or shear instabilities).

1 Introduction

Mixing efficiency (Γ) quantifies the change in background potential energy due to mixing relative to the turbulent kinetic energy expended through mixing (Gregg et al., 2018)

$$\Gamma = \frac{J_b}{\varepsilon}, \tag{1}$$

where J_b is buoyancy flux and ε is turbulent kinetic energy dissipation rate. The buoyancy flux can be expressed as

$$J_b = -\frac{g}{\rho_0}\overline{\rho' w'} = -\frac{g}{\rho_0} K_\rho \frac{d\overline{\rho}}{dz} = K_\rho N^2, \tag{2}$$

where g is gravitational acceleration, ρ density and ρ_0 mean density, w vertical velocity, K_ρ turbulent diapycnal diffusivity, N buoyancy frequency, overlines denote a mean quantity and primes fluctuations from the mean. For a homogeneous, isotropic, stratified, vertically sheared steady flow, the turbulent kinetic energy production is equivalent to (Osborn, 1980)

$$P = \varepsilon - J_b \quad \Leftrightarrow \quad \overline{u'w'}\frac{\partial U}{\partial z} = \varepsilon - K_\rho N^2. \tag{3}$$

The flux Richardson number R_f is defined as the ratio between the buoyancy flux and the production of turbulent kinetic energy

$$R_f = \frac{J_b}{P} = \frac{(g/\rho_0)\overline{\rho' w'}}{\overline{u'w'}\partial U/\partial z}. \tag{4}$$

The Osborn (1980) turbulence model, valid for shear driven mixing but not for convective or double diffusive mixing, assumes $K_\theta = K_\rho$ and

$$\Gamma_t = \frac{K_\rho N^2}{\varepsilon}, \tag{5}$$

with Γ_t the shear driven turbulence mixing efficiency. In this case R_f can also be expressed as

$$R_f = \frac{\Gamma_t}{1 + \Gamma_t}. \tag{6}$$

The Osborn and Cox (1972) relation for turbulent thermal diffusivity K_θ

$$K_\theta = \frac{\chi}{2(\partial\overline{\theta}/\partial z)^2}, \tag{7}$$

where χ is the dissipation rate of temperature variance, gives the relation for the dissipation flux coefficient Γ_d (also referred to as dissipation ratio, dissipation coefficient, or mixing coefficient; Oakey 1985; Moum 1997; Ruddick et al. 1997; Gregg et al. 2018)

$$\Gamma_d = \Gamma_t \frac{K_\theta}{K_\rho} = \frac{\chi N^2}{2\varepsilon \left(\frac{\partial \theta}{\partial z}\right)^2}. \tag{8}$$

The dissipation flux coefficient Γ_d is commonly inferred from measurements as an equivalent of the mixing efficiency, assuming that convective and double diffusive mixing are negligible compared to mechanically driven turbulent mixing. Double diffusive mixing is driven by the release of potential energy through buoyancy due to a destabilising temperature or salinity vertical gradient, a process thus fundamentally different from turbulent mixing. Equation (8) is equivalent to

$$\Gamma_d = \left(\frac{R_f}{1 - R_f}\right) \frac{K_\theta}{K_\rho}. \tag{9}$$

In the case of pure double diffusion ($\frac{\partial U}{\partial z} = 0$ and $K_\theta \neq K_\rho$), Γ_d is not representative of the mixing efficiency: $\Gamma_t = \frac{R_f}{1-R_f}$=-1 and the mixing efficiency is $\Gamma_{DD} = -\frac{K_\theta}{K_\rho}$ (St. Laurent and Schmitt, 1999).

R_f has generally been adopted as a universal constant derived from the estimation that one sixth of the turbulent kinetic energy produced is converted into potential energy, the rest being lost through friction, resulting in $\Gamma_t = 0.2$ (Osborn, 1980). However, more recent studies have revealed a great variability in mixing efficiency, inferred from field measurements (van Haren et al., 1994; Moum, 1997; Ruddick et al., 1997; Inoue et al., 2007; Sundfjord et al., 2007; Davis and Monismith, 2011; Dunckley et al., 2012; Ijichi and Hibiya, 2018; Monismith et al., 2018), direct numerical simulations (DNS, Slinn and Riley, 1996, 1998; Smyth et al., 2001; Peltier and Caulfield, 2003; Umlauf and Burchard, 2011; Mashayek and Peltier, 2013; Chalamalla and Sarkar, 2015; Salehipour and Peltier, 2015; Mashayek et al., 2017), as well as laboratory experiments (Ivey and Nokes, 1989; Strang and Fernando, 2001). Notably, the numerical simulations of Shih et al. (2005), based on the laboratory experiments of Barry et al. (2001), showed that the mixing efficiency may be expressed as a function of the turbulence intensity Re_b, defined as the ratio of the destabilising effect of turbulence to the stabilising effect of stratification and viscosity

$$Re_b = \frac{\varepsilon}{\nu N^2}, \tag{10}$$

where ν is kinematic viscosity and N buoyancy frequency. Bouffard and Boegman (2013) refined the Shih et al. (2005) parameterisation with a validation against in-situ measurements, distinguishing between distinct turbulent regimes (with Γ increasing with increasing Re_b in the buoyancy controlled regime up to $Re_b = 8.5$, where it reaches a plateau at 0.2 in the transitional regime, before decreasing at $Re_b = 400$ in the energetic regime). A dependency on the turbulence intensity was also revealed by a variety of mixing efficiency estimates from field measurements, direct numerical simulations and laboratory experiments alike (e.g. Monismith et al., 2018), and from measurements collected in the Sicily Channel (Vladoiu et al., 2019). Nevertheless, the mixing efficiency does not depend solely on Re_b. Gregg et al. (2018) suggest that mixing efficiency is likely driven by more than one non-dimensional parameter, but also advocate that the variety of methods used to asses mixing efficiency and the associated uncertainties do not allow a compelling characterisation of this dependence, hence recommend to keep the conventional 0.2 hypothesis.

This study builds on the results presented in Vladoiu et al. (2019) and addresses the variability of the dissipation flux coefficient Γ_d as a proxy for the mixing efficiency with 134 microstructure profiles collected in the Western Mediterranean basin east of $5°E$. The same methods are employed for the entire dataset, allowing for a consistent analysis over a wider range of turbulence levels and dynamical regimes than previously reported, thus proving that the observed variability is not due to computation or sampling discrepancies. The dependency of the dissipation flux coefficient on turbulence intensity and other parameters suggested in the literature is explored, and the consequences of the observed variability on the large scale circulation is discussed with respect to quantifying turbulent fluxes and changes in water mass properties.

2 Data and Methods

2.1 Data

The analysis is based on the first full-depth microstructure profiles sampled in the Western Mediterranean Sea with a Vertical Microstructure Profiler (VMP6000), described in Ferron et al. (2017). The microstructure dataset used in this study comprises 118 profiles sampled during 5 cruises (14 profiles during Venus2 in June 2013, 24 during Ichnussa13 in October 2013, 28 during Medocc2014 in March-April 2014, 12 during Emso01 in June-July 2014, and 40 during Ichnussa14 in November 2014) including the 16 profiles from the Sicily Channel described in Vladoiu et al. (2019). An additional 16 profiles sampled in the Sicily Channel during DYNAS (15 of which between May 22^{nd}-25^{th} 2018 and 1 of which on September 23^{rd} 2018) with the same instrument were also included. The profiles locations are shown in Figure 1. Collocated current data from LADCP (Lowered Acoustic Doppler Current Profiler, RDI WH 300 kHz, bin size 4 m) were also available for 85 of the 134 VMP profiles. The dissipation rates of turbulent kinetic energy (ε) and of thermal variance (χ) were inferred from the VMP measurements with 1 m and 2 m vertical resolution, as described in Ferron et al. (2017) and Vladoiu et al. (2019), respectively.

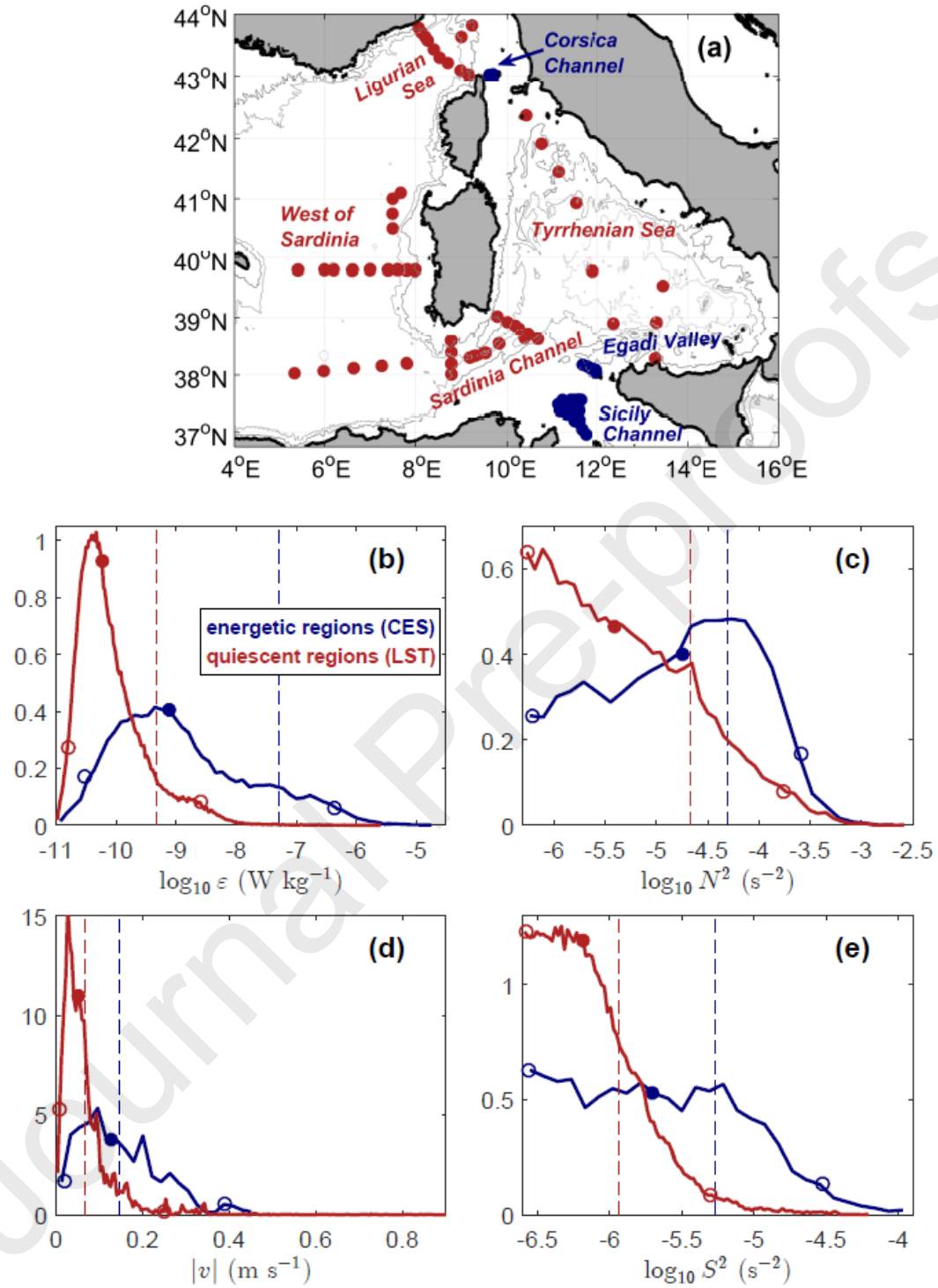

Figure 1: Stations locations (a) colour coded for the two types of regions: energetic regions (blue) - Corsica Channel, Egadi Valley and Sicily Channel (CES), and quiescent regions (red) - Ligurian Sea, West of Sardinia, Sardinia Channel, and Tyrrhenian Sea (LST).
Probability density function of dissipation rate (b), buoyancy frequency squared (c), current velocity (d) and velocity vertical shear (e), for the Corsica Channel, Egadi Valley and Sicily Channel energetic regions (CES, blue) and for the Ligurian Sea, West of Sardinia, Sardinia Channel, and Tyrrhenian Sea quiescent regions (LST, red); the dashed lines indicate the mean, the filled circles indicate the median, and the empty circles indicate the 2.5 and 97.5 percentiles.

2.2 Dissipation flux coefficient as an estimate of the mixing efficiency for mechanically driven turbulent mixing

The dissipation flux coefficient was computed from the microstructure measurements based on Equation (8). Vertical averaging was performed over varying length segments, corresponding to the turbulent patches extensions and as a function of the Ozmidov scale, as described in Vladoiu et al. 2019 (58% equal to 2 m, 41% between 2 and 10 m, and 1% greater than 10 m). The dissipation flux coefficient variability was assessed by employing the same methods as in Vladoiu et al. (2019). The vertical shear squared $S^2 = (\partial u/\partial z)^2 + (\partial v/\partial z)^2$ was computed from LADCP profiles sampled from the CTD rosette and collocated with the VMP profiles, and the buoyancy frequency N^2 was computed from the VMP Seabird CTD using sorted density profiles. The Richardson number Ri was calculated as $Ri = N^2/S^2$, from N and S lowpass first-order Butterworth filtered over 20 m. Shear instabilities at smaller vertical scales are likely not resolved due to resolution limitations. Noise levels of 5 $\times 10^{-7}$ s^{-2}, 2.5 $\times 10^{-7}$ s^{-2}, and 10^{-11} W kg^{-1} were applied to N^2, S^2 and ε, respectively. The imposed noise limit on buoyancy frequency restricts the analysis roughly to the upper 1000 m, 95 (99) % of the Γ_d estimates being at depths shallower than 606 (758) m and just 0.3% below 1000 m.

Regions where double diffusive instabilities may develop in conditions of weak turbulence and favourable temperature and salinity gradients were excluded from the analysis. In the Mediterranean Sea, structures indicative of double diffusion such as temperature or salinity "steps" are common (e.g. Onken and Brambilla, 2003; Carniel et al., 2008). In particular, the very saline and warm intermediate waters (comprised mostly of Levantine Intermediate Water) relative to the deep and surface waters may satisfy the stability conditions required for the development of salt fingers and diffusive convection, respectively: if warm and salty waters overlay cool and fresh waters, double diffusive salt fingers may develop, while in the case of cool and fresh waters overlaying warm and salty waters, double diffusive convection may develop (Schmitt, 1994). The water column stability to double diffusion was assessed depending on the temperature and salinity vertical gradients using the Turner angle Tu (Ruddick, 1983)

$$Tu = tan^{-1}\frac{-\alpha\partial_z T - \beta\partial_z S}{-\alpha\partial_z T + \beta\partial_z S}, \tag{11}$$

where α and β are the thermal expansion and saline contraction coefficients, respectively. Tu indicates the relative contribution of salinity and temperature to the stability of a layer with

respect to double diffusion processes, allowing a classification in four regimes (Ruddick, 1983): favourable for double diffusion - salt finger ($45° < Tu < 90°$) and diffusive convection ($-90° < Tu < -45°$) regimes, and unfavourable for double diffusion - stable ($|Tu| < 45°$) and overturn ($|Tu| > 90°$) regimes. If the preconditioning for double diffusive processes is satisfied in this respect, it does not necessarily imply that double diffusion occurs. In the following, "salt finger regime" and "double diffusive regime" are used only in reference to the Turner angle and the sign of the temperature and salinity vertical gradients (positive temperature and salinity gradients in the case of salt fingers, and negative in the case of diffusive convection), and do not imply that double diffusive processes dominate. Double diffusion was assumed to prevail over mechanically driven turbulence only if: Re_b<25 (Stillinger et al., 1983; Padman and Dillon, 1987; Gregg, 1988), $\chi/\varepsilon > 1$ (Alford and Pinkel, 2000), and $-90° < Tu < -45°$ or $45° < Tu < 90°$. This occurred for 4% of the vertical segments (or 6% of the sub-sample restricted to $Re_b < 25$), equivalent to 467 instances of diffusive convection and 337 of salt fingers. These occurrences were excluded from the analysis on Γ_d variability. Double diffusive mixing relative to mechanically driven mixing was highest at the least turbulent stations in the Tyrrhenian Sea and West of Sardinia (5-6% of the total number of vertical segments).

3 Results

The profiles were classified into two types of regions where similar dynamical regimes are expected to prevail (Figure 1):

- energetic regions - Corsica Channel, Egadi Valley and Sicily Channel (CES), which are shallow regions where the flow is constricted by the bathymetry, with mean $\varepsilon = 5.2 \times 10^{-8}$ W kg^{-1}, mean $N^2 = 4.9 \times 10^{-5}$ s^{-2}, mean current velocities of 0.15 m s^{-1}, mean $S^2 = 5.3 \times 10^{-6}$ s^{-2}.

- quiescent regions - Ligurian Sea, West of Sardinia, Sardinia Channel, and Tyrrhenian Sea (LST), which are comparatively more offshore and less prone to flow-topography interactions, with mean $\varepsilon = 4.7 \times 10^{-10}$ W kg^{-1}, mean $N^2 = 2.2 \times 10^{-5}$ s^{-2}, mean current velocities of 7 cm s^{-1}, mean $S^2 = 1.2 \times 10^{-6}$ s^{-2}.

A contrast was observed between CES and LST, with larger mean and median dissipation rate, buoyancy frequency, current velocity and vertical shear at CES than at LST (Figure 1). Moreover, Ferron et al. (2017) reported a higher range of dissipation rate variability between cruises below 100 m at CES than at LST. The energetic regions comprise 44 profiles and 28% of the total 18469 segments over which Γ_d was computed, and the quiescent regions 90 profiles and 72% of the segments (see Table 1 for numbers of profiles and percentages for each region).

	Region	Number of profiles	% of total number of segments
Energetic regions (CES)	Corsica Channel	6	3
	Sicily Channel	32	20
	Egadi Valley	6	5
Quiescent regions (LST)	Ligurian Sea	11	9
	Sardinia Channel	35	29
	West of Sardinia	32	23
	Tyrrhenian Sea	12	11

Table 1: Number of microstructure profiles in each region shown in Figure 1; percentage of segments over which Γ_d was computed in each region relative to total number of segments in all regions.

The dependency of Γ_d on Re_b was investigated (in $\log_{10}$ space) and compared to the Bouffard and Boegman (2013) parameterisation (Γ_{BB13}), for the two types of regions (Figure 2). At LST, only 1.7% of the observations occur at Re_b>1000, compared to 16% at CES. At CES, and consistently with the parameterisation, Γ_d showed distinct linear dependencies on Re_b subject to the Re_b range. Γ_d was on average systematically larger than Γ_{BB13}. Γ_d exhibits a plateau for the mean values in the transitional Re_b regime with $8.5 \leq Re_b < 400$ defined by Bouffard and Boegman (2013) that here extends up to $Re_b = 10^4$, consistent with the behaviour observed in the Sicily Channel and described in Vladoiu et al. 2019 (this plateau is still observed when disregarding the profiles from the Sicily Channel). Around $Re_b = 10^4$, a transition to a dependency described by $Re_b^{-1/2}$ occurs, which is consistent with Monismith et al. (2018). This transition therefore appears far after the end of the Bouffard and Boegman (2013) transitional regime. Conversely, at LST Γ_d decreased on average continuously and almost linearly with increasing Re_b, a behaviour that differs markedly from the 4 distinct regimes predicted by the Bouffard and Boegman (2013) parameterisation (Figure 2). In the energetic regime with $Re_b \geq 400$, Γ_d is on average half an order of magnitude larger than Γ_{BB13}.

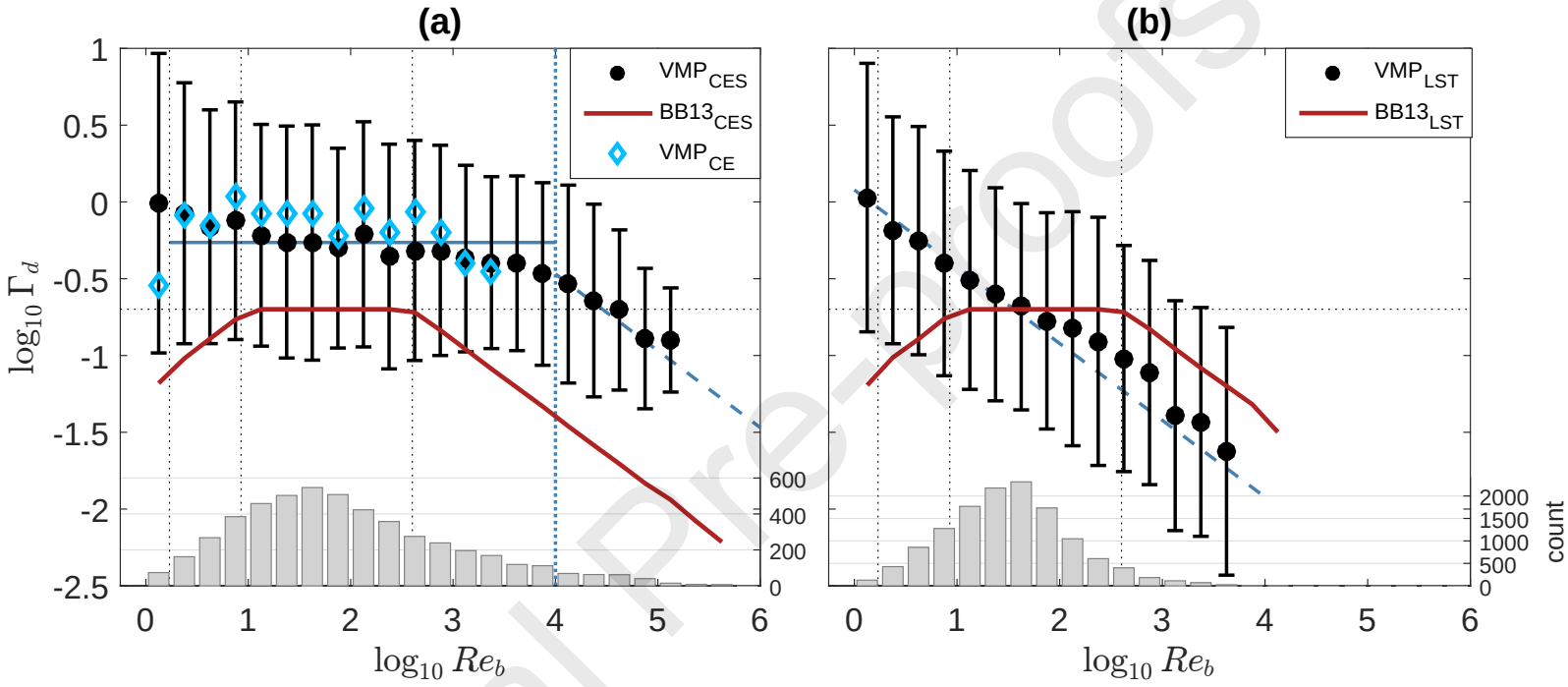

Figure 2: $\log_{10}\Gamma_d$ (black circles) averaged in bins of $\log_{10} Re_b$, for the Corsica Channel, Egadi Valley and Sicily Channel energetic regions (CES, a), only for the Corsica Channel and Egadi Valley regions (CE, a, blue diamonds), and for the Ligurian Sea, West of Sardinia, Sardinia Channel, and Tyrrhenian Sea quiescent regions (LST, b); Γ_{BB13} (red curves); ΔRe_b=0.25 in $\log_{10}$ space; delimitations of the Bouffard and Boegman (2013) turbulent regimes: molecular for $Re_b < 1.7$, buoyancy controlled for $1.7 \leq Re_b < 8.5$, transitional for $8.5 \leq Re_b < 400$, energetic for $Re_b \geq 400$ (dotted black lines); black bars show the standard deviation; grey bars show the number of occurrences in each Re_b bin (only bins with at least 10 occurrences are shown); $\log_{10}\Gamma_d$ averaged over $1.7 \leq Re_b < 10^4$ (solid blue line, a), $Re_b = 10^4$ (vertical dotted blue line) at which the transition from a plateau to a slope proportional to $Re_b^{-1/2}$ occurs (Monismith et al. 2018, dashed blue line, a and b).

Monismith et al. (2018) reviewed a collection of datasets that revealed different behaviours of the Richardson flux number (directly related to the dissipation flux coefficient, Equation (6)) as a function of turbulence intensity (Figure 3). Many datasets exhibit a saturation of R_f, illustrated by a plateau such as that of the Bouffard and Boegman (2013) transitional turbulence intensity regime, followed by a decrease in R_f with increasing Re_b. However, the critical Re_b at which R_f starts to decrease differs between studies. In particular, the strongly sheared, strongly stratified estuarine case presented in Holleman et al. (2016) and characterised by high dissipation rates resembles the energetic regions (CES), in that R_f starts to decrease with increasing Re_b far after the Bouffard and Boegman (2013) limit of 400 (Figure 3). On the other hand, the almost linear decrease in R_f with increasing Re_b in the transitional regime illustrated by the quiescent regions (LST) was consistent between field measurements, direct numerical simulations and laboratory experiments alike. Interestingly, the R_f curves from the two types of regions in the Western Mediterranean roughly frame the upper and lower bounds of the different datasets in the composite plot. Therefore, Figure 3 further suggests that the mixing efficiency variability is likely not governed only by the turbulence intensity.

The distribution of Γ_d in (ε, N^2) space is also contrasting between CES and LST (Figure 4). The bulk of the values at CES is restricted to a smaller parameter space than at LST, and corresponds to mean N^2 and ε roughly one order of magnitude larger. There is some variability in Γ_d along Re_b isolines at both CES and LST, but no clear consistent pattern emerges between CES and LST, suggesting either lacking statistical significance or that the (ε, N^2) space is insufficient to fully describe the mixing efficiency variability and that further parameters are involved.

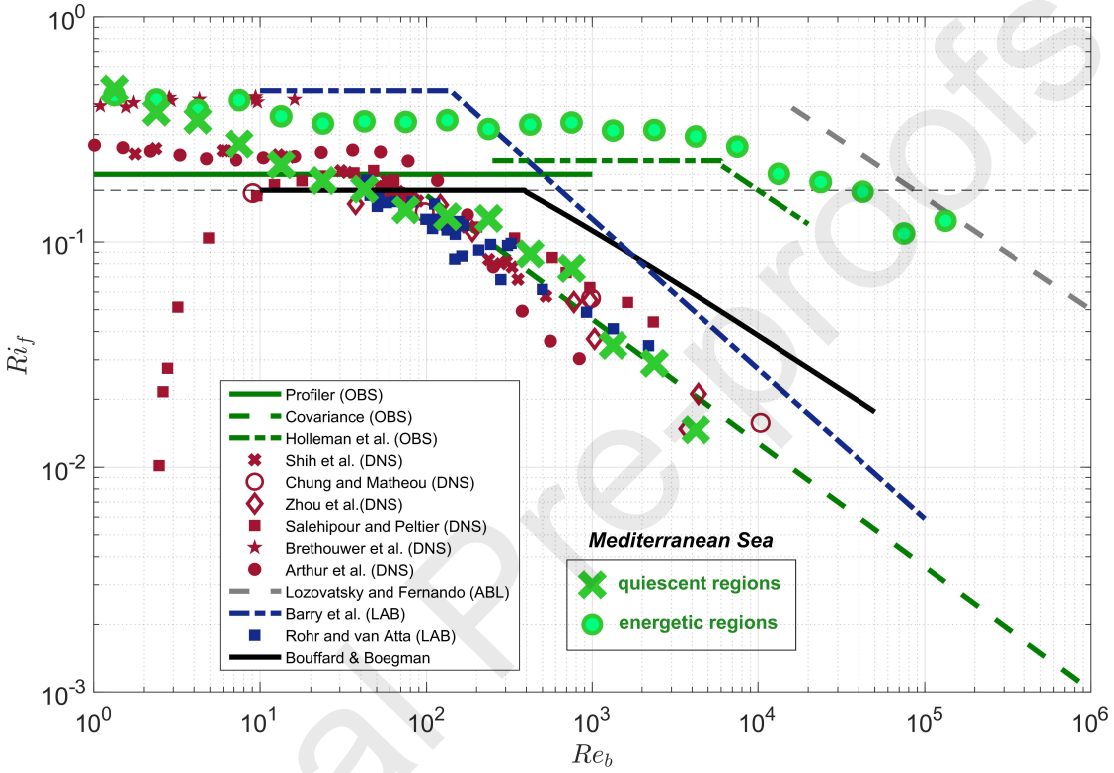

Figure 3: Composite plot of the median Richardson flux number as a function of turbulence intensity from several studies (after Monismith et al. 2018, incorporating an additional dataset by Brethouwer et al. 2007; data courtesy of Stephen Monismith) based on: field measurements (green lines - OBS), direct numerical simulations (red symbols - DNS), laboratory experiments (blue line and squares - LAB), atmospheric boundary layer measurements (grey line - ABL). The Bouffard and Boegman (2013) parameterisation is also shown (black line), and the binned medians from the Western Mediterranean Sea corresponding to Figure 2 are superimposed (green circles - energetic regions and green crosses - quiescent regions).

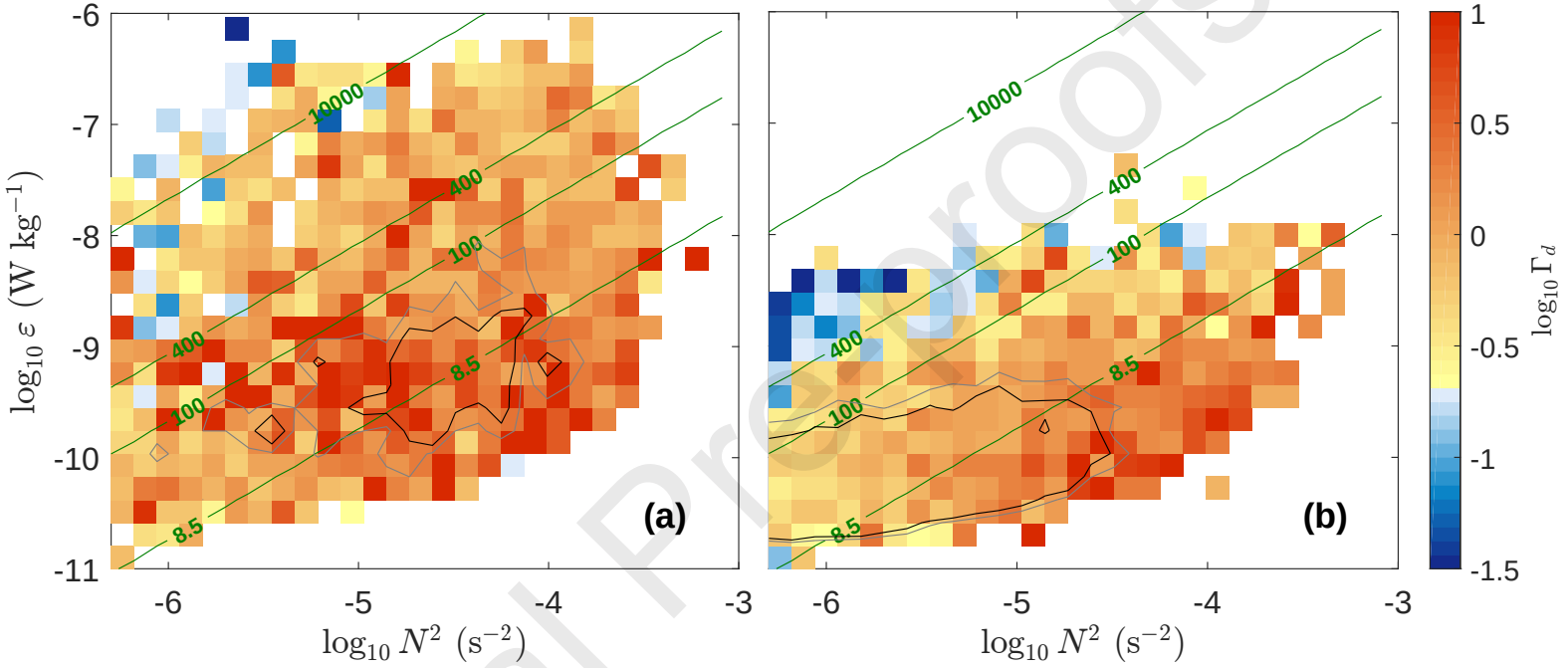

Figure 4: Bin averaged Γ_d (N^2, ε) for the Corsica Channel, Egadi Valley and Sicily Channel energetic regions (CES, a) and for the Ligurian Sea, West of Sardinia, Sardinia Channel, and Tyrrhenian Sea quiescent regions (LST, b); Re_b (green contours); 0.2 and 0.15 contours of the probability density function (black and gray, respectively); $\Delta\log_{10} N^2$=0.12, $\Delta\log_{10}\varepsilon$=0.21; note the colour map transition from blue to yellow at Γ_d=0.2; only bins with at least 3 occurrences are shown.

The dependency of Γ_d, ε, N^2, S^2, Ri, and K_θ on Re_b was investigated for the four water column stability regimes with respect to the Turner angle. As explained in Section 2.2, the following disregards segments with prevailing double diffusion (indicated for reference in (Tu, Re_b) space in Figures 5 a and 6 a) and refers to the diffusive convection and salt finger regimes only in terms of the temperature and salinity gradients; moreover, the segments are mostly restricted to the upper 1000 m. Γ_d varied significantly not only as a function of Re_b, but also depending on the Tu regime. At both CES and LST, Γ_d was highest in the stable and diffusive convection regimes, and significantly lower in the salt finger regime (Figures 5 a and 6 a), consistent with Inoue et al. (2007). At CES, median Γ_d at $Re_b < 400$ was 0.62 in the stable regime, 0.75 in the diffusive convection regime and 0.3 in the salt finger regime, while at $Re_b \geq 400$ median values were 0.43, 0.55 and 0.29, respectively. Conversely, at LST, median Γ_d at $Re_b < 400$ was 0.3 in the stable regime, 0.31 in the diffusive convection regime and 0.13 in the salt finger regime, while at $Re_b \geq 400$ median values were 0.11, 0.11 and 0.03, respectively. This may be related to the variability of K_θ, which shows a consistent pattern between CES and LST: K_θ increases on average with increasing Re_b but is larger in the diffusive convective regime than in the salt finger regime (Figures 5 f and 6 f). This asymmetry is likely not due to the criterion $Re_b < 25$ used to distinguish double diffusion (a bias induced by prevailing double diffusion would imply $K_\theta \neq K_\rho$), as it extends well beyond this value. The S^2 and N^2 variability in (Tu, Re_b) space differed greatly between CES and LST, suggesting the presence of water masses with different properties and dynamics as outlined previously. S^2 was overall higher for CES (Figure 5 d) than for LST (Figure 6 d), and strong shear occurred mostly in the stable and diffusive convection regimes and at all Re_b at CES. Conversely, at LST the strongest shear occurred in the stable regime at low Re_b, and S^2 decreased uniformly with increasing Re_b for all the regimes. This indicates that at LST the increase in Re_b is mainly due to the decrease in stratification at low dissipation rate, rather than to the strong production of turbulence by the mean shear. At Re_b between 8.5 and 400, N^2 was much larger at CES (Figure 5 c) than at LST (Figure 6 c), especially in the diffusive convection regime but also in the stable regime. There was a contrast between the water column stability regimes also for Ri, at both CES and LST: Ri was larger in the diffusive convective regime than in the salt finger regime (Figures 5 e and 6 e). Ri was larger at LST than at CES in the transitional Re_b regime for all Tu regimes due to the dominance of weaker stratification at LST and despite larger shear at CES. A contrast in the transitional Re_b regime between CES and LST was also observed for S^2 and K_θ, with higher values at CES than at LST.

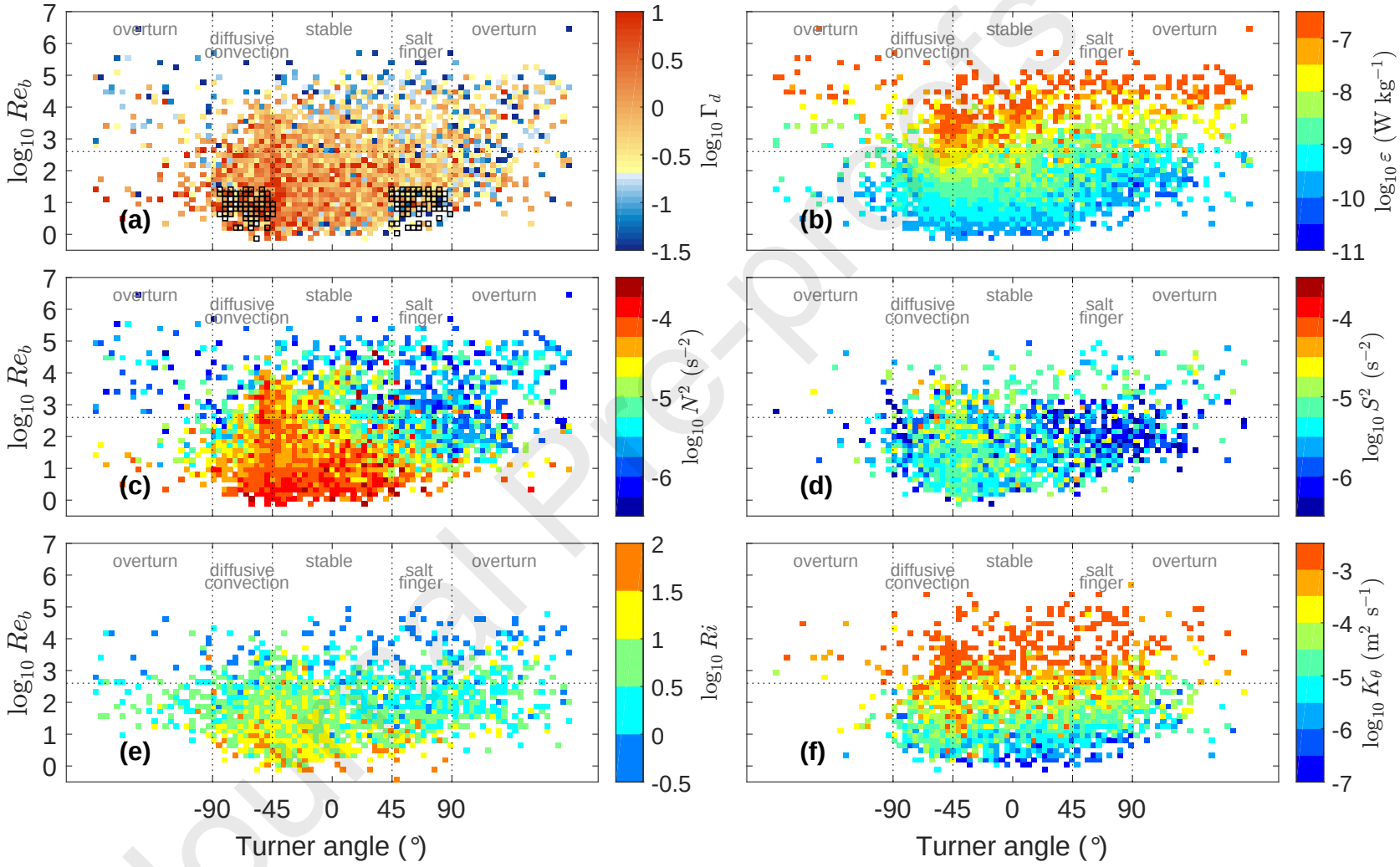

Figure 5: Bin averages in (Tu, Re_b) space for the Corsica Channel, Egadi Valley and Sicily Channel energetic regions (CES) (ΔTu=4°, $\Delta \log_{10} Re_b$=0.17) of: Γ_d (a), ε (b), N^2 (c), S^2 (d), Ri (e), and K_θ (f). Note same y axis for (a)-(f).
The Tu water column stability regimes refer to the T and S vertical gradients (negative T and S gradients for the diffusive convection regime, and positive T and S gradients for the salt finger regime), and do not necessarily imply that double diffusion occurs. The (Tu, Re_b) bins where double diffusion is potentially prevalent relative to mechanically-driven mixing are restricted to Re_b<25, $\chi/\varepsilon > 1$, and $-90° < Tu < -45°$ or $45° < Tu < 90°$, and are indicated in (a) by the black squares. The horizontal dashed black line indicates Re_b=400.

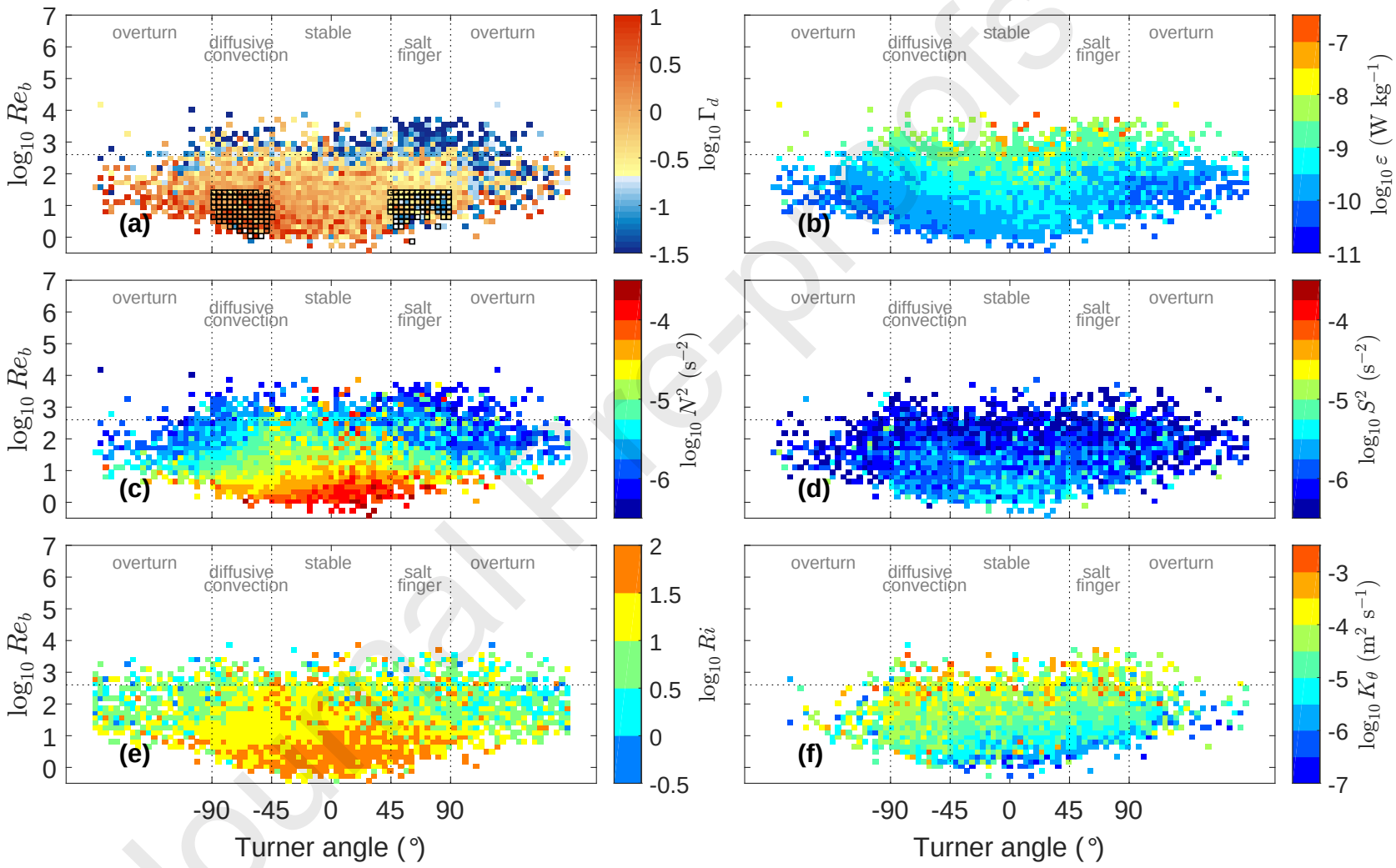

Figure 6: Same as Figure 5, but for the Ligurian Sea, West of Sardinia, Sardinia Channel, and Tyrrhenian Sea quiescent regions (LST).

The behaviour of Γ_d as a function of Ri in the Sicily Channel (Vladoiu et al., 2019) was found to be relatively well described on average by the parameterisation suggested by Venayagamoorthy and Koseff (2016), based on the direct numerical simulations of Shih et al. (2005) which predicts a constant value at $Ri > 1$. Moreover, the Γ_d dependency for Ri up to ≈ 1 was in agreement with predictions by several numerical simulations and laboratory experiments of shear instability (Stretch et al., 2010; Schaad and Venayagamoorthy, 2017; Zhou et al., 2017). However, for the complete Western Mediterranean dataset, no clear dependency of Γ_d on Ri was observed for either CES or LST (Figure 7). This inconclusive dependency is consistent with the results of Monismith et al. (2018) based on a combination of datasets. It is possible that Ri is not computed at small enough scales from the measurements, or that shear instability is not a sufficiently dominant mechanism to shape a dependence on Ri.

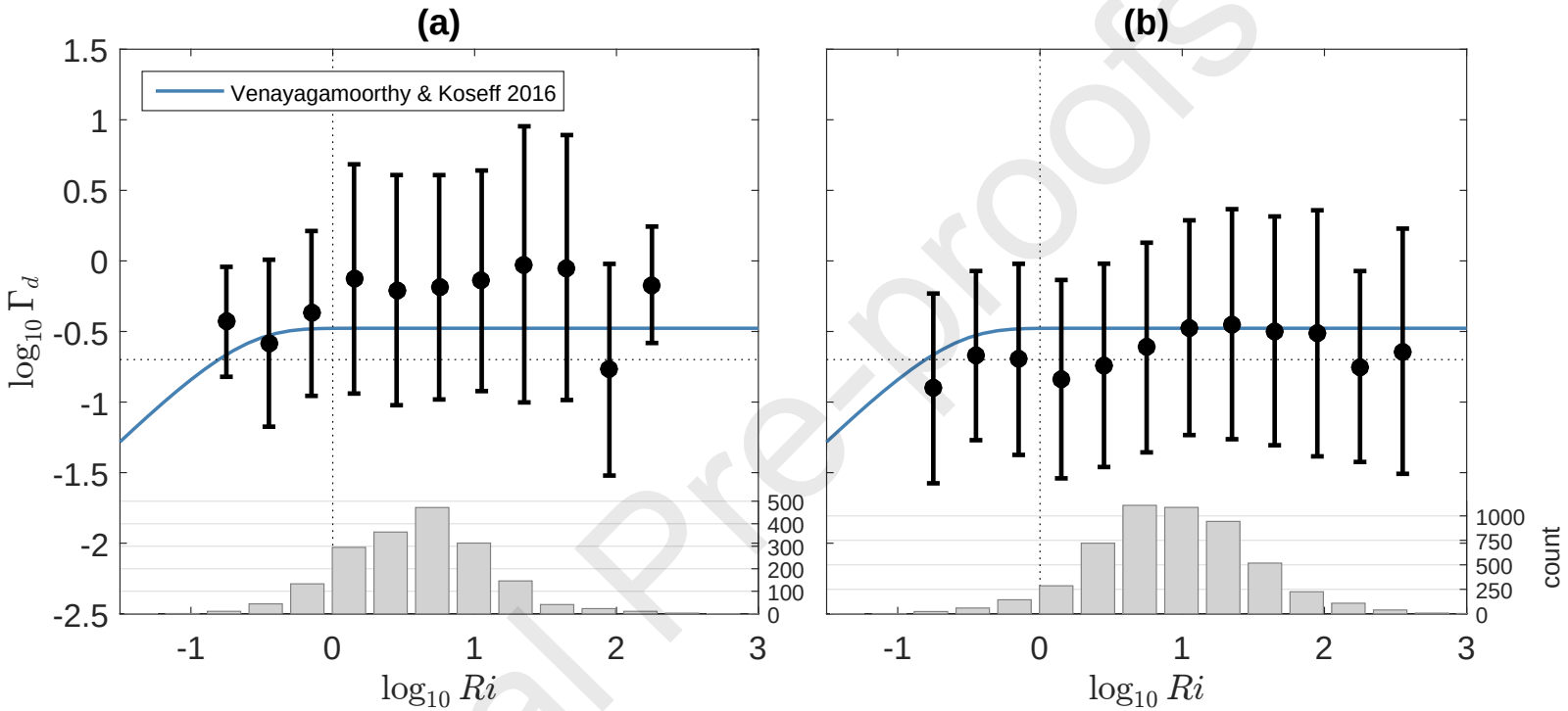

Figure 7: Γ_d (black circles) averaged in bins of Ri, for the Corsica Channel, Egadi Valley and Sicily Channel energetic regions (CES, a), and for the Ligurian Sea, West of Sardinia, Sardinia Channel, and Tyrrhenian Sea quiescent regions (LST, b); standard deviation for each bin (error bars); grey bars show the number of occurrences in each Ri bin (only bins with at least 10 occurrences are shown); $\Delta Ri = 0.3$ in $\log_{10}$ space; the parameterisation suggested by Venayagamoorthy and Koseff (2016) is shown for comparison (blue line).

A dependency of the mixing efficiency on the ratio between the Ozmidov scale (L_O) and the Thorpe scale (L_T) has been suggested based on scaling analysis and laboratory experiments (Ivey and Imberger, 1991), direct numerical simulations (Smyth et al., 2001; Garanaik and Venayagamoorthy, 2019), and oceanic measurements (Smyth et al., 2001; Ijichi and Hibiya, 2018; Ijichi et al., 2020). The Thorpe scale quantifies the extent of a turbulent patch $L_T = \langle \delta_T^2 \rangle^{1/2}$, where δ_T is the vertical displacement from a depth sorted density profile, and the Ozmidov length scale $L_O = \langle \varepsilon \rangle^{1/2} \langle N \rangle^{-3/2}$ represents the maximum vertical extent of a turbulent overturn in the presence of buoyancy forces (angle brackets denote averages over a turbulent patch). The ratio L_O/L_T was computed for each turbulent patch with L_O and L_T greater than 1 m. A ratio close to one is expected for shear driven mixing (Scotti, 2015) and was only found at CES concurrently with large Re_b. At LST $L_O \ll L_T$, consistent with previous results in the ocean interior and suggesting that convective mixing may occur (Mater et al., 2015). Γ_d decreased on average with increasing L_O/L_T, with a redder slope at LST than at CES (Figure 8). However, the low number of resolved turbulent patches due to the noise threshold imposed on N and to the restriction $L_O > 1$ m does not allow a robust comparison with the previously suggested scalings in the same parameter space.

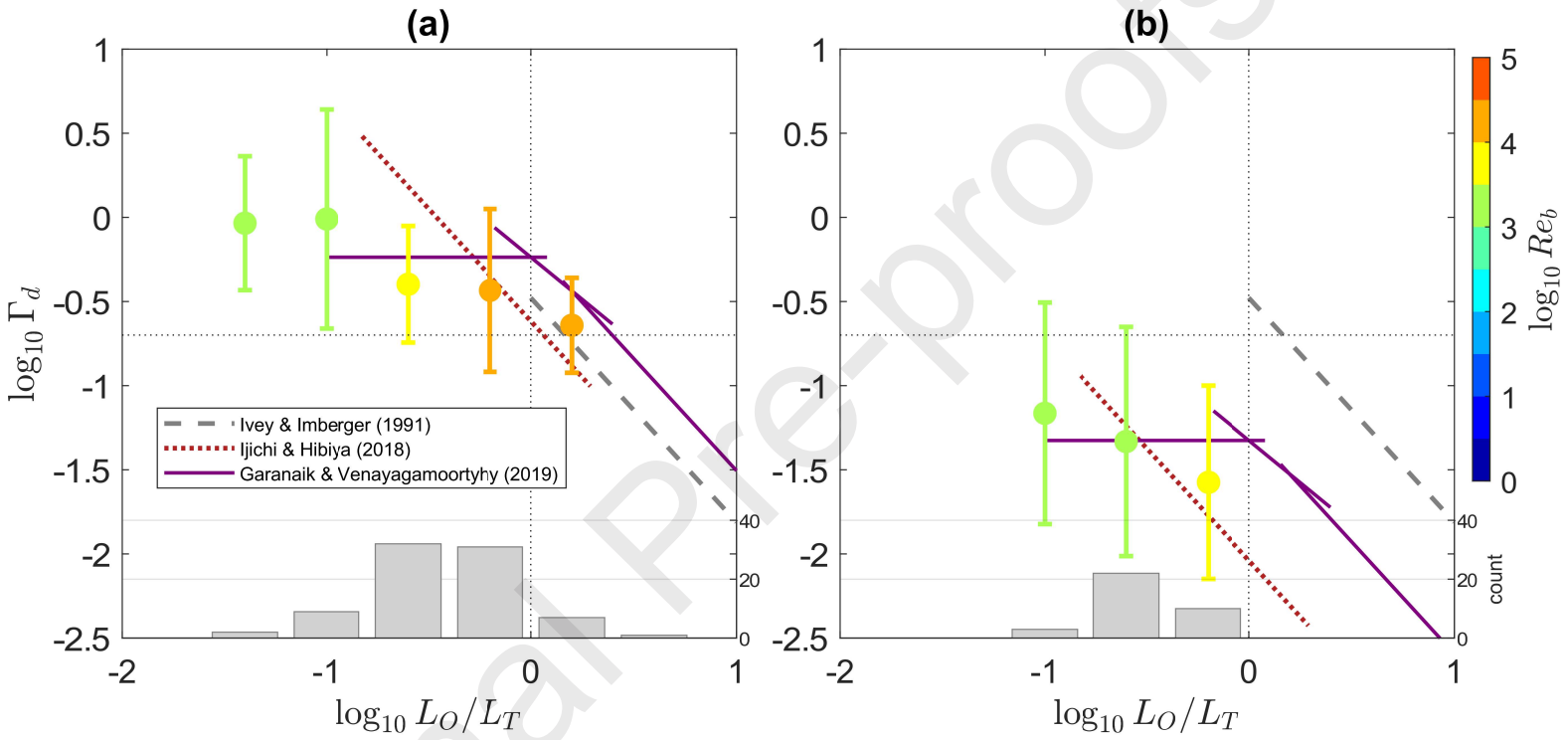

Figure 8: Γ_d (circles) averaged in bins of L_O/L_T, for the Corsica Channel, Egadi Valley and Sicily Channel energetic regions (CES, a), and for the Ligurian Sea, West of Sardinia, Sardinia Channel, and Tyrrhenian Sea quiescent regions (LST, b); averaged Re_b in bins of L_O/L_T (colour); standard deviation for each bin (error bars); grey bars show the number of turbulent patches considered in each L_O/L_T bin; the scalings suggested by Ivey and Imberger (1991); Ijichi and Hibiya (2018); Garanaik and Venayagamoorthy (2019) are shown for comparison (dashed gray, dotted red, and solid purple curves, respectively).

The contrasting dissipation flux coefficient between CES and LST, with smaller Γ_d in the quiescent compared to energetic regions, implies significant differences in vertical turbulent diffusive fluxes and water mass transformations between the two types of regions. Moreover, large ε concurrent with large Γ_d in the energetic regions result in a larger buoyancy flux $J_b = \varepsilon\Gamma_d$ than in the quiescent regions, suggesting that most of the diapycnal mixing occurs at CES. Intermediate waters were identified based on vertical profiles and T-S diagrams between $28.8 \leq \sigma_0 \leq 29.1$ kg m^{-3}, corresponding to 59% of the total observations at CES and 89% at LST, and with 90% of the occurrences between roughly 175 and 526 m depth at CES and between 130 and 640 m depth at LST. Diapycnal diffusivity K_ρ estimated from Γ_d (Equation (5)) for $28.8 \leq \sigma_0 \leq 29.1$ kg m^{-3} has a mean (median) of 3.7×10^{-3} (8.2×10^{-5}) m^2 s^{-1} at CES and 5.8×10^{-5} (9×10^{-6}) m^2 s^{-1} at LST. Moreover, the mean K_ρ parameterised as a function of Re_b following Bouffard and Boegman (2013) is smaller by a factor of 24 and 3 for the mean value at CES and LST, respectively, than K_ρ inferred from Γ_d. This further underlines the importance of microstructure measurements for more accurate estimates of vertical turbulent diffusive fluxes.

4 Conclusions and discussion

Microstructure profiles sampled in the Western Mediterranean basin east of $5°E$ were classified into two types of dynamical regions: energetic (Corsica Channel, Egadi Valley and Sicily Channel) and quiescent (Ligurian Sea, around Sardinia, and Tyrrhenian Sea). The currents, vertical shear, stratification and dissipation were stronger in the energetic than in the quiescent regions.

The dissipation flux coefficient variability as a function of turbulence intensity also differed greatly between the two types of regions, especially at Re_b between 10 and 10^4: while on average Γ_d exhibits a plateau in the energetic regions, in the quiescent regions Γ_d decreases almost linearly (in $\log_{10}$ space) with increasing Re_b. The Bouffard and Boegman (2013) prediction lies in between these two curves. A plateau was also found in some previous studies but its extension is variable (e.g. Holleman et al., 2016). The decrease in Γ_d with increasing Re_b was suggested to be induced by boundary effects, however this dependency is exhibited precisely in the offshore quiescent regions, away from coastal boundaries and bathymetric features. The Bouffard and Boegman (2013) parameterisation is based on numerical simulations (Shih et al., 2005) and laboratory experiments (Barry et al., 2001), and was validated with in-situ measurements from Lake Erie. The range of parameters reproduced in these simulations and experiments may be more similar to those found in the energetic, well stratified regions. The in-situ data from Lake Erie and from other studies that showed a similar Γ_d behaviour may also be more representative of the conditions in the energetic regions. For instance in Lake Erie high dissipation rates occur in a sharp thermocline as a result of strong internal Poincaré waves (Bouffard et al., 2012). The Western Mediterranean dataset covers a wide spectrum of dynamical conditions and a large range of turbulence intensities, comparable with the Monismith et al. (2018) compilation but with the advantage of a uniform method being employed, thus removing the possibility that the different observed dependencies would be attributed to different processing methods. As noted by Monismith et al. (2018), a dependency of the mixing efficiency on Re_b does exist but it is most probably not the only parameter governing its variability. The Richardson number, at least computed at the large vertical scales imposed by the current measurement limitations, does not seem to govern the variability of Γ_d.

An apparent dependence of Γ_d on the water column stability regime was observed, with higher dissipation flux coefficient for mechanically driven mixing in the case of the diffusive

convection favourable regime than in the case of the salt finger favourable regime. A similar contrast was also evidenced by Inoue et al. (2007). This may indicate a bias in the Osborn-Cox method in the case of the regimes favourable for double diffusion, but where mechanical mixing is assumed to prevail. More specifically, when the background stratification is favourable for diffusive convection, the transition between diffusive convective mixing and mechanical mixing for increasing turbulence intensity is likely not abrupt, and there may remain a signature of diffusive convection in the temperature variance of the turbulent regime, resulting in a bias in the Osborn-Cox estimation. However, this contrast persists even at $Re_b \gg 25$, and these stability regimes also identify water masses subjected to contrasted shear and stratification conditions. This point could be addressed with the use of process oriented direct numerical simulations or laboratory experiments. In addition, studies based on microconductivity measurements could be conducted in parallel, to asses the Osborn-Cox method in regimes favourable to double diffusion, especially in regions where the stratification is highly influenced by salinity as is the case in the Mediterranean Sea. This method is much less frequently used (e.g. Nash and Moum, 2002; Walter et al., 2014; Holleman et al., 2016) due to sensor resolution and noise issues.

Based on the Buckingham π theorem for dimensional analysis and considering the variables turbulent kinetic energy, turbulent kinetic energy dissipation rate, buoyancy frequency, vertical velocity shear, viscosity, and thermal and saline molecular diffusivity, described by their respective length and time scales, Gregg et al. (2018) estimated that the mixing efficiency could be characterised by 5 dimensionless parameters. Numerical simulations suggest that the mixing efficiency variability depends at least on a quantity describing the stratification and on one describing the level of turbulence (Gregg et al., 2018). A caveat of numerical simulations as those performed by Shih et al. (2005) is that large Re_b concurs with weak stratification, which is not the case everywhere in the ocean, therefore N^2 should be considered as an independent factor (Gregg et al., 2018). A collapse of the dissipation flux coefficient was indeed observed for low N^2 in the Western Mediterranean dataset. Moreover, numerical simulations generally only reproduce one idealised mixing mechanism (most often Kelvin-Helmholtz sheared turbulence), which is not necessarily representative of the complex assortment of interacting processes at different stages of development in the ocean. While $\Gamma_t = 0.2$ is a good approximation for steady state shear-driven mixing with no initial overturning (e.g. Caulfield, 2020), pre-existent turbulence strongly affects the mixing efficiency of a shear instability (Kaminski and Smyth, 2019). In DNS, the age of a turbulent mixing event induced by shear instability was shown to be equivalent to the ratio of

the Ozmidov to the Thorpe scales (e.g. Smyth et al., 2001). Based on estimates inferred from observations, Mashayek et al. (2017) found a behaviour of the mixing efficiency as a function of the turbulence intensity that is similar to that exhibited by the Mediterranean quiescent regions for young turbulence, while the case of older turbulence rather resembles the behaviour observed in the energetic regions. Similarly, Cyr and Van Haren (2016) found higher mixing efficiency estimated from finescale density (mean 0.36) during energetic periods associated with the collapse of internal bores and younger turbulence, than during less energetic periods of decaying turbulence (mean 0.2). As for ocean measurements, little consistency exists between observational datasets. This is likely partly due to measurement and method related limitations and uncertainties (e.g. Gregg et al., 2018). Consistent with Monismith et al. (2018), no clear dependence on Ri was evident for the Western Mediterranean dataset, possibly due to the inadequate vertical resolution of classical CTD/LADCP measurements used to infer Ri; this question could be addressed by employing more accurate current meters with a high vertical resolution of the order of 1 m.

Mixing efficiency is generally parameterised in order to estimate diapycnal diffusivity from microstructure measurements and subsequently compute vertical turbulent diffusive fluxes. The diapycnal diffusivity estimates based on the dissipation flux coefficient confirmed that the localised Western Mediterranean energetic regions with a strong bathymetry constricted flow are hotspots for vertical turbulent mixing of intermediate water mass properties. Advection in particular helps sustain the strong stratification in the energetic regions and thus contributes to maintain a high mixing efficiency, in contrast to the quiescent, less stratified regions. The average diapycnal eddy diffusivity on the global oceanic scale was estimated from energy and transport budgets at 10^{-4} m^2 s^{-1} (Munk, 1966; Munk and Wunsch, 1998). However, mixing is strongly heterogeneous and local values differ by orders of magnitude (Wunsch and Ferrari, 2004; Waterhouse et al., 2014). Ocean global circulation models are very sensitive to the way mixing efficiency and diapycnal diffusivity are represented, and more accurate parameterisations need to be developed and implemented (De Lavergne et al., 2016; Mashayek et al., 2017; Cimoli et al., 2019). This study further suggests that models should employ a non-constant mixing efficiency and should distinguish between quiescent regions where the mixing efficiency is significantly below 0.2, and energetic regions with mixing efficiency well above 0.2. Considering that most of the ocean volume has similar characteristics to the quiescent regions, this difference may cancel out on a large scale but be locally important. The relative significance of the localised mixing hot spots should therefore be more thoroughly addressed. To this end, the mixing efficiency

variability depending on the mechanisms that drive mixing needs to be further investigated.

Acknowledgements

The authors thank Stephen Monismith for providing the data used in Figure 3 and two anonymous reviewers for their suggestions which helped improve the manuscript. The authors also wish to thank all crew members of the R/V Urania (CNR-ISMAR), as well as Alberto Ribotti (CNR-IAMC, Oristano) and Stefania Sparnocchia (CNR-ISAMR, Trieste), Chief Scientists during the Ichnussa2013 and Emso01 cruises, respectively. The data used in this paper were acquired within the framework of a project funded by CNR-ISMAR, LOCEAN, LOPS, and the HyMeX (HYdrological cycle in The Mediterranean EXperiment) and INSU-MISTRALS (Mediterranean Integrated STudies at Regional And Local Scales) programs. The microstructure profiler was funded by the French Agence Nationale de la Recherche (ANR) through Grant ANR-310 JC05-50690 and by the French Research Institute for Exploitation of the Sea (IFREMER). The authors also acknowledge the support of the European Commission through the H2020 Framework Programme JERICO NEXT under grant agreement No. 654410.

References

Alford, M., and R. Pinkel, 2000: Patterns of turbulent and double-diffusive phenomena: Observations from a rapid-profiling microconductivity probe. *Journal of Physical Oceanography*, **30 (5)**, 833–854, doi:https://doi.org/10.1175/1520-0485(2000)030<0833:POTADD>2.0.CO;2.

Barry, M. E., G. N. Ivey, K. B. Winters, and J. Imberger, 2001: Measurements of diapycnal diffusivities in stratified fluids. *Journal of Fluid Mechanics*, **442**, 267–291, doi:https://doi.org/10.1017/S0022112001005080.

Bouffard, D., and L. Boegman, 2013: A diapycnal diffusivity model for stratified environmental flows. *Dynamics of Atmospheres and Oceans*, **61**, 14–34, doi:http://dx.doi.org/10.1016/j.dynatmoce.2013.02.002.

Bouffard, D., L. Boegman, and Y. R. Rao, 2012: Poincaré wave–induced mixing in a large lake. *Limnology and oceanography*, **57 (4)**, 1201–1216, doi:https://doi.org/10.4319/lo.2012.57.4.1201.

Brethouwer, G., P. Billant, E. Lindborg, and J.-M. Chomaz, 2007: Scaling analysis and simulation of strongly stratified turbulent flows. *Journal of Fluid Mechanics*, **585**, 343–368, doi:https://doi.org/10.1017/S0022112007006854.

Carniel, S., M. Sclavo, L. Kantha, and H. Prandke, 2008: Double–diffusive layers in the Adriatic Sea. *Geophysical Research Letters*, **35 (2)**, doi:https://doi.org/10.1029/2007GL032389.

Caulfield, C., 2020: Layering, instabilities, and mixing in turbulent stratified flows. *Annual Review of Fluid Mechanics*, **53**, doi:https://doi.org/10.1146/annurev-fluid-042320-100458.

Chalamalla, V. K., and S. Sarkar, 2015: Mixing, dissipation rate, and their overturn-based estimates in a near-bottom turbulent flow driven by internal tides. *Journal of Physical Oceanography*, **45 (8)**, 1969–1987, doi:10.1175/JPO-D-14-0057.1.

Cimoli, L., P. C. Colm-cille, H. L. Johnson, D. P. Marshall, A. Mashayek, A. C. N. Garabato, and C. Vic, 2019: Sensitivity of deep ocean mixing to local internal tide breaking and mixing efficiency. *Geophysical Research Letters*, doi:https://doi.org/10.1029/2019GL085056.

Cyr, F., and H. Van Haren, 2016: Observations of small–scale secondary instabilities during the shoaling of internal bores on a deep–ocean slope. *Journal of Physical Oceanography*, **46 (1)**, 219–231, doi:https://doi.org/10.1175/JPO-D-15-0059.1.

Davis, K. A., and S. G. Monismith, 2011: The modification of bottom boundary layer turbulence and mixing by internal waves shoaling on a barrier reef. *Journal of physical oceanography*, **41 (11)**, 2223–2241, doi:10.1175/2011JPO4344.1.

De Lavergne, C., G. Madec, J. Le Sommer, A. Nurser, and A. Naveira Garabato, 2016: The impact of a variable mixing efficiency on the abyssal overturning. *Journal of Physical Oceanography*, **46 (2)**, 663–681, doi:10.1175/JPO-D-14-0259.1.

Dunckley, J., J. Koseff, J. Steinbuck, S. Monismith, and A. Genin, 2012: Comparison of mixing efficiency and vertical diffusivity models from temperature microstructure. *Journal of Geophysical Research: Oceans*, **117 (C10)**, doi:10.1029/2012JC007967.

Ferron, B., P. Bouruet Aubertot, Y. Cuypers, K. Schroeder, and M. Borghini, 2017: How important are diapycnal mixing and geothermal heating for the deep circulation of the Western Mediterranean? *Geophysical Research Letters*, **44 (15)**, 7845–7854, doi:10.1002/2017GL074169.

Garanaik, A., and S. K. Venayagamoorthy, 2019: On the inference of the state of turbulence and mixing efficiency in stably stratified flows. *Journal of Fluid Mechanics*, **867**, 323–333, doi:https://doi.org/10.1017/jfm.2019.142.

Gregg, M., 1988: Mixing in the thermohaline staircase east of Barbados. *Elsevier Oceanography Series*, **46**, 453–470, doi:https://doi.org/10.1016/S0422-9894(08)70564-6.

Gregg, M., E. D'Asaro, J. Riley, and E. Kunze, 2018: Mixing Efficiency in the Ocean. *Annual Review of Marine Science*, **(0)**, doi:https://doi.org/10.1146/annurev-marine-121916-063643.

Holleman, R., W. Geyer, and D. Ralston, 2016: Stratified turbulence and mixing efficiency in a salt wedge estuary. *Journal of Physical Oceanography*, **46 (6)**, 1769–1783, doi:10.1175/JPO-D-15-0193.1.

Ijichi, T., and T. Hibiya, 2018: Observed variations in turbulent mixing efficiency in the deep ocean. *Journal of Physical Oceanography*, **48 (8)**, 1815–1830, doi:https://doi.org/10.1175/

JPO-D-17-0275.1.

Ijichi, T., L. St. Laurent, K. L. Polzin, and J. M. Toole, 2020: How variable is mixing efficiency in the abyss? *Geophysical Research Letters*, **47 (7)**, e2019GL086 813, doi:https://doi.org/10.1029/2019GL086813.

Inoue, R., H. Yamazaki, F. Wolk, T. Kono, and J. Yoshida, 2007: An estimation of buoyancy flux for a mixture of turbulence and double diffusion. *Journal of Physical Oceanography*, **37 (3)**, 611–624, doi:https://doi.org/10.1175/JPO2996.1.

Ivey, G., and R. Nokes, 1989: Vertical mixing due to the breaking of critical internal waves on sloping boundaries. *Journal of Fluid Mechanics*, **204**, 479–500, doi:10.1017/S0022112089001849.

Ivey, G. N., and J. Imberger, 1991: On the nature of turbulence in a stratified fluid. Part I: The energetics of mixing. *Journal of Physical Oceanography*, **21 (5)**, 650–658, doi:https://doi.org/10.1175/1520-0485(1991)021<0650:OTNOTI>2.0.CO;2.

Kaminski, A., and W. Smyth, 2019: Stratified shear instability in a field of pre-existing turbulence. *Journal of Fluid Mechanics*, **862**, 639–658, doi:10.1017/jfm.2018.973.

Mashayek, A., and W. R. Peltier, 2013: Shear-induced mixing in geophysical flows: does the route to turbulence matter to its efficiency? *Journal of Fluid Mechanics*, **725**, 216–261, doi:10.1017/jfm.2013.176.

Mashayek, A., H. Salehipour, D. Bouffard, C. Caulfield, R. Ferrari, M. Nikurashin, W. Peltier, and W. Smyth, 2017: Efficiency of turbulent mixing in the abyssal ocean circulation. *Geophysical Research Letters*, doi:10.1002/2016GL072452.

Mater, B. D., S. K. Venayagamoorthy, L. St. Laurent, and J. N. Moum, 2015: Biases in Thorpe-scale estimates of turbulence dissipation. Part I: Assessments from large–scale overturns in oceanographic data. *Journal of Physical Oceanography*, **45 (10)**, 2497–2521, doi:https://doi.org/10.1175/JPO-D-14-0128.1.

Monismith, S. G., J. R. Koseff, and B. L. White, 2018: Mixing efficiency in the presence of stratification: When is it constant? *Geophysical Research Letters*, doi:https://doi.org/10.1029/2018GL077229.

Moum, J. N., 1997: Efficiency of mixing in the main thermocline. *Oceanographic Literature Review*, **1 (44)**, 16.

Munk, W., and C. Wunsch, 1998: Abyssal recipes II: Energetics of tidal and wind mixing. *Deep Sea Research Part I: Oceanographic Research Papers*, **45 (12)**, 1977–2010, doi:https://doi.org/10.1016/S0967-0637(98)00070-3.

Munk, W. H., 1966: Abyssal recipes. *Deep Sea Research and Oceanographic Abstracts*, Elsevier, Vol. 13, 707–730, doi:https://doi.org/10.1016/0011-7471(66)90602-4.

Nash, J. D., and J. N. Moum, 2002: Microstructure estimates of turbulent salinity flux and the dissipation spectrum of salinity. *Journal of Physical Oceanography*, **32 (8)**, 2312–2333, doi:https://doi.org/10.1175/1520-0485(2002)032<2312:MEOTSF>2.0.CO;2.

Oakey, N., 1985: Statistics of mixing parameters in the upper ocean during JASIN Phase 2. *Journal of Physical Oceanography*, **15 (12)**, 1662–1675, doi:https://doi.org/10.1175/1520-0485(1985)015<1662:SOMPIT>2.0.CO;2.

Onken, R., and E. Brambilla, 2003: Double diffusion in the Mediterranean Sea: Observation and parameterization of salt finger convection. *Journal of Geophysical Research: Oceans*, **108 (C9)**, doi:https://doi.org/10.1029/2002JC001349.

Osborn, T., 1980: Estimates of the local rate of vertical diffusion from dissipation measurements. *Journal of Physical Oceanography*, **10 (1)**, 83–89, doi:https://doi.org/10.1175/1520-0485(1980)010<0083:EOTLRO>2.0.CO;2.

Osborn, T., and C. Cox, 1972: Oceanic fine structure. *Geophysical & Astrophysical Fluid Dynamics*, **3 (1)**, 321–345, doi:https://doi.org/10.1080/03091927208236085.

Padman, L., and T. M. Dillon, 1987: Vertical heat fluxes through the Beaufort Sea thermohaline staircase. *Journal of Geophysical Research: Oceans*, **92 (C10)**, 10 799–10 806, doi:10.1029/JC092iC10p10799.

Peltier, W. R., and C. P. Caulfield, 2003: Mixing efficiency in stratified shear flows. *Annual Review of Fluid Mechanics*, **35 (1)**, 135–167, doi:10.1146/annurev.fluid.35.101101.161144.

Ruddick, B., 1983: A practical indicator of the stability of the water column to double–diffusive

activity. *Deep Sea Research Part A. Oceanographic Research Papers*, **30 (10)**, 1105–1107, doi:https://doi.org/10.1016/0198-0149(83)90063-8.

Ruddick, B., D. Walsh, and N. Oakey, 1997: Variations in apparent mixing efficiency in the North Atlantic Central Water. *Journal of Physical Oceanography*, **27 (12)**, 2589–2605, doi:https://doi.org/10.1175/1520-0485(1997)027<2589:VIAMEI>2.0.CO;2.

Salehipour, H., and W. Peltier, 2015: Diapycnal diffusivity, turbulent prandtl number and mixing efficiency in boussinesq stratified turbulence. *Journal of Fluid Mechanics*, **775**, 464–500, doi:10.1017/jfm.2015.305.

Schaad, S., and S. Venayagamoorthy, 2017: Direct numerical simulations of stably stratified decaying unforced turbulence. *Computers & Fluids*, doi:https://doi.org/10.1016/j.compfluid.2017.05.022.

Schmitt, R., 1994: Double diffusion in oceanography. *Annual Review of Fluid Mechanics*, **26 (1)**, 255–285, doi:https://doi.org/10.1146/annurev.fl.26.010194.001351.

Scotti, A., 2015: Biases in Thorpe–scale estimates of turbulence dissipation. Part II: energetics arguments and turbulence simulations. *Journal of Physical Oceanography*, **45 (10)**, 2522–2543, doi:https://doi.org/10.1175/JPO-D-14-0092.1.

Shih, L., J. Koseff, G. Ivey, and J. Ferziger, 2005: Parameterization of turbulent fluxes and scales using homogeneous sheared stably stratified turbulence simulations. *Journal of Fluid Mechanics*, **525**, 193–214, doi:10.1017/S0022112004002587.

Slinn, D. N., and J. Riley, 1998: Turbulent dynamics of a critically reflecting internal gravity wave. *Theoretical and computational fluid dynamics*, **11 (3-4)**, 281–303, doi:10.1007/s001620050094.

Slinn, D. N., and J. J. Riley, 1996: Turbulent mixing in the oceanic boundary layer caused by internal wave reflection from sloping terrain. *Dynamics of Atmospheres and Oceans*, **24 (1-4)**, 51–62, doi:10.1016/0377-0265(95)00425-4.

Smyth, W. D., J. N. Moum, and D. R. Caldwell, 2001: The efficiency of mixing in turbulent patches: Inferences from direct simulations and microstructure observations. *Journal of Physical Oceanography*, **31 (8)**, 1969–1992, doi:https://doi.org/10.1175/1520-0485(2001)031<1969:

TEOMIT>2.0.CO;2.

St. Laurent, L., and R. Schmitt, 1999: The contribution of salt fingers to vertical mixing in the North Atlantic Tracer Release Experiment. *Journal of Physical Oceanography*, **29 (7)**, 1404–1424, doi:https://doi.org/10.1175/1520-0485(1999)029<1404:TCOSFT>2.0.CO;2.

Stillinger, D., K. Helland, and C. Van Atta, 1983: Experiments on the transition of homogeneous turbulence to internal waves in a stratified fluid. *Journal of Fluid Mechanics*, **131**, 91–122, doi:https://doi.org/10.1017/S0022112083001251.

Strang, E. J., and H. J. S. Fernando, 2001: Entrainment and mixing in stratified shear flows. *Journal of Fluid Mechanics*, **428**, 349–386, doi:https://doi.org/10.1017/S0022112000002706.

Stretch, D., J. Rottman, S. Venayagamoorthy, K. Nomura, and C. Rehmann, 2010: Mixing efficiency in decaying stably stratified turbulence. *Dynamics of atmospheres and oceans*, **49 (1)**, 25–36, doi:https://doi.org/10.1016/j.dynatmoce.2008.11.002.

Sundfjord, A., I. Fer, Y. Kasajima, and H. Svendsen, 2007: Observations of turbulent mixing and hydrography in the marginal ice zone of the Barents Sea. *Journal of Geophysical Research: Oceans*, **112 (C5)**, doi:10.1029/2006JC003524.

Umlauf, L., and H. Burchard, 2011: Diapycnal transport and mixing efficiency in stratified boundary layers near sloping topography. *Journal of physical oceanography*, **41 (2)**, 329–345, doi:10.1175/2010JPO4438.1.

van Haren, H., N. Oakey, and C. Garrett, 1994: Measurements of internal wave band eddy fluxes above a sloping bottom. *Journal of Marine Research*, **52 (5)**, 909–946, doi:10.1357/0022240943076876.

Venayagamoorthy, S. K., and J. R. Koseff, 2016: On the flux Richardson number in stably stratified turbulence. *Journal of Fluid Mechanics*, **798**, doi:https://doi.org/10.1017/jfm.2016.340.

Vladoiu, A., P. Bouruet-Aubertot, Y. Cuypers, B. Ferron, K. Schroeder, M. Borghini, S. Leizour, and S. B. Ismail, 2019: Mixing efficiency from microstructure measurements in the Sicily Channel. *Ocean Dynamics*, doi:10.1007/s10236-019-01274-2.

Walter, R., M. Squibb, C. Woodson, J. Koseff, and S. Monismith, 2014: Stratified turbulence in the nearshore coastal ocean: Dynamics and evolution in the presence of internal bores. *Journal of Geophysical Research: Oceans*, **119 (12)**, 8709–8730, doi:10.1002/2014JC010396.

Waterhouse, A. F., and Coauthors, 2014: Global patterns of diapycnal mixing from measurements of the turbulent dissipation rate. *Journal of Physical Oceanography*, **44 (7)**, 1854–1872, doi:https://doi.org/10.1175/JPO-D-13-0104.1.

Wunsch, C., and R. Ferrari, 2004: Vertical mixing, energy, and the general circulation of the oceans. *Annu. Rev. Fluid Mech.*, **36**, 281–314, doi:10.1146/annurev.fluid.36.050802.122121.

Zhou, Q., J. Taylor, and C. Caulfield, 2017: Self–similar mixing in stratified plane Couette flow for varying Prandtl number. *Journal of Fluid Mechanics*, **820**, 86–120, doi:https://doi.org/10.1017/jfm.2017.200.

Declaration of interests

☒ The authors declare that they have no known competing financial interests or personal relationships that could have appeared to influence the work reported in this paper.

☐The authors declare the following financial interests/personal relationships which may be considered as potential competing interests: